Brazilian Journal of Physics
On-line version ISSN 1678-4448

Braz. J. Phys. vol. 27 n. 4 São Paulo Dec. 1997

http://dx.doi.org/10.1590/S0103-97331997000400007

Photoionization Cross Sections and Asymmetry Parameters for Ethylene

L.M. Brescansin*, M.-T. Lee**, L.E. Machado[1], M.A.P. Lima*, and V. McKoy[2]

* *Instituto de Física, UNICAMP, 13083-970 Campinas, SP, Brazil*

** *Departamento de Química, UFSCar, 13565-905 São Carlos, SP, Brazil*

[1] *Departamento de Física, UFSCar, 13565-905 São Carlos, SP, Brazil*

[2] *A. A. Noyes Laboratory of Chemical Physics, Caltech, Pasadena, Ca., 91125*

Received August 12, 1997

We present the results of applications of the iterative Schwinger variational method to obtain photoionization cross sections and phoelectron angular distributions for ionization out of the four outermost valence orbitals $1b_{3u}$, $1b_{3g}$, $3a_g$ and $1b_{2u}$ of ethylene for photon energies ranging from near threshold to 30 eV. The observed resonance-like maxima in the cross sections for ionization of the $1b_{3g}$ and $3a_g$ orbitals are reproduced in our calculations. The disagreement between our cross sections and the experimental data for the $1b_{3u}$ orbital below 17 e V is attributed to autoionization, which is not accounted for in our calculations.

I. Introduction

Although there is a considerable increasing interest on the investigation of rotationally resolved photoionization spectroscopy [1-4], conventional photoelectron studies in molecules can still provide valuable insight into the underlying photoionization dynamics, *e.g.*, the role of shape resonances in photoelectron spectra [5,6] and of non-Franck-Condon vibrational distributions of photoions [7,8]. On the theoretical point of view, calculations of

photoionization spectra require quantitative estimates of the photoelectron matrix elements which accurately incorporate the angular momentum coupling present in molecular photoelectron wavefunctions.

In our previous studies we have derived these photoionization matrix elements using Hartree-Fock photoelectron orbitals obtained from a numerical solution of the Lippmann-Schwinger equation using the Schwinger variational iterative method (SVIM) (Ref. [9]). This procedure has proven to be numerically robust and capable of providing a quantitative description of the photoionization dynamics in molecular systems studied to date [4]. Although this method was developped in the early eighties and has been applied to studies of photoionization of linear systems [10-12], it still constitutes one of a few tools for carrying out *ab initio* calculations of cross sections and asymmetry parameters for photoionization of nonlinear polyatomic molecules. For the photoionization of such molecules, even at the static-exchange (SE) level of approximation, the application of SVIM has been limited to two systems [13,14]. The comparison between the calculated results in the exact SE level with the experimental data would provide information on the role played by important physical effects, *e.g.,* multichannel coupling, correlation-polarization effects, etc., not included in the calculations. In addition, the SE calculation represents the first step towards rotationally resolved photioinization studies.

In this paper we present the results of a theoretical study of photoionization of ethylene. Specifically, we report vibrationally and rotationally unresolved photoionization cross sections and photoelectron asymmetry parameters for the $1b_{3u}$, $1b_{3g}$, $3a_g$ and $1b_{2u}$ valence orbitals of ethylene. Over the years, photoionization of C_2H_4 has been the subject of a few experimental and theoretical investigations. Partial photoionization cross sections for several valence orbitals have been measured by Grimm *et al*. [15] and by Brennan *et al*. [16], while the photoelectron angular distributions were reported by Mehaffy *et al.* [17]. More recently, the photoionization cross sections and asymmetry parameters for the C_{1s} orbital of ethylene were studied by Kilcoyne *et al.* [18]. On the theoretical side, the partial cross sections and asymmetry parameters for some valence and inner-valence orbitals were both calculated only by Grimm [19], using the continuum multiple-scattering Xa ($CMSX_a$) method. The Stieltjes-Tchebycheff moment theory (STMT) method has been used by Galasso [20] and Farren *et al.* [21] to study the photoionization cross sections of C_2H_4, although the latter has reported only the partial cross sections for the photoionization of the $3a_g$ orbital. However, it is well known that the STMT is unable to provide the asymmetry parameters of the photoelectrons. Therefore, the present work is the first *ab initio* calculation of both partial cross sections and asymmetry parameters for several valence and inner-valence orbitals of this molecule.

The paper is organized as follows. In the next section we briefly review the method used for obtaining the photoelectron orbitals and matrix elements along with some numerical details of the calculation. In section III we present our calculated photoionization cross sections and photoelectron asymmetry parameters and compare them with selected experimental data and other available theoretical results. Finally, in section IV we summarize our conclusions.

II. Theory and Calculation

Details of the procedure have been given elsewhere [13,14] and only a few essential aspects will be discussed here. The photoelectron angular distribution averaged over molecular orientations is given by:

$$\frac{d\sigma^{(L,V)}}{d\Omega_{\hat{k}}} = \frac{\sigma^{(L,V)}}{4\pi}\left[1 + \beta_{\hat{k}}^{(L,V)} P_2(\cos\theta)\right], \quad (1)$$

where $s^{(L,V)}$ is the total photoionization cross section, obtained with the length (L) or velocity (V) form of the dipole moment operator. For nonlinear molecules, $s^{(L,V)}$ is given by :

$$\sigma^{(L,V)} = \frac{4\pi^2 E}{3c} \sum_{p\mu lhv} |I^{p\mu(L,V)}_{lhv}|^2, \quad (2)$$

where E is the photon energy, p is one of the irreducible representations (IR) of the symmetry group of the molecule and h distinguishes between different bases for the same IR corresponding to the same value of l. The index m labels components of vectors belonging to the same IR and v designates components of the dipole moment operator.

In Eq. (1), $\beta_{\hat{k}}^{(L,V)}$ is the asymmetry parameter and can be written as:

$$\beta_{\hat{k}}^{(L,V)} = \frac{3}{5}\frac{1}{\sum_{p\mu lhv}|I^{p\mu}_{lhv}|^2}(1100|20)\sum_{\substack{p\mu lhvmm_\nu \\ p'\mu' l'h'v'm'm_\nu'}}(-1)^{m'-m_\nu}I^{p\mu(L,V)}_{lhv}\ I^{p\mu(L,V)*}_{l'h'v'}\ b^{p\mu}_{lhm}\ b^{p'\mu'}_{l'h'm'}\times$$

$$b^{p_\nu\mu_\nu}_{lvm\nu}\ b^{p_\nu'\mu_\nu'}_{l'v'm\nu'}\ [(2l+1)(2l'+1)]^{\frac{1}{2}}(11\text{-}m_\nu m_\nu|2M')(l'100|20)(l'1\text{-}m'm|2\text{-}M'). \quad (3)$$

The $b^{p\mu}_{lhm}$ are the expansion coefficients of the symmetry-adapted functions in terms of the usual spherical harmonics [22], while the $I^{p\mu(L,V)}_{lhv}$ appearing in Eqs. (2) and (3) are the partial-wave components of the dynamical coefficients $I^{(L,V)}_{\vec{k},\hat{n}}$ which can be written as [9]:

$$I^{(L)}_{\vec{k},\hat{n}} = (k)^{1/2} < \Psi_i|\ \vec{r}\ \cdot\hat{n}\ |\Psi^{(-)}_{\vec{k}} > \quad (4)$$

and

$$I^{(V)}_{\vec{k},\hat{n}} = \frac{(k)^{1/2}}{E} < \Psi_i|\ \vec{\nabla}\ \cdot\hat{n}\ |\Psi^{(-)}_{\vec{k}} >, \quad (5)$$

respectively. In Eqs. (4) and (5), Y_i is the target ground state wave function, $\Psi^{(-)}_{\vec{k}}$ the final state (incoming-wave normalized) wavefunction for the system (ion plus photoelectron), $\hat{n}$ a unit vector in the direction of polarization of the radiation and $\vec{k}$ the photoelectron momentum.

In the present study, Y_i is a Hartree-Fock (HF) wavefunction. The final state is described by a single electronic configuration in which the ionic core orbitals are constrained to be identical to those of the initial ground state. In this approximation, the photoelectron orbital is a solution of the one-electron Schrödinger equation :

$$\left[-\frac{1}{2}\nabla^2+V_{N-1}(\vec{r}\ ;\ \vec{R}\ )+\frac{k^2}{2}\right]\phi_{\vec{k}}(\vec{r}\ )=0\ , \quad (6)$$

where V_{N-1} is the static-exchange potential of the molecular ion and $\phi_{\vec{k}}(\vec{r})$ satisfies appropriate boundary conditions. To proceed, Eq. (6) is rewritten in an integral form, the Lippmann-Schwinger equation, which is then solved using an iterative procedure based on the Schwinger variational principle.

For the SCF calculation of the ground state we used the standard [9s5p,3s] contracted Gaussian basis of Dunning [23] augmented with three uncontracted s functions (a = 0.0473, 0.0125 and 0.0045), three p functions (a = 0.0365, 0.0125 and 0.0035), and one d function (a = 0.75), on the carbon nuclei and two p functions (a = 0.5571 and 0.1296) on the hydrogens. At the experimental equilibrium geometry of $R_{(C\text{-}C)}$ = 2.5133 a.u., $R_{(C\text{-}H)}$ = 2.0333 a.u., and $q_{(H\text{-}C\text{-}H)}$ = 116.6°, this basis set gives an SCF energy of -78.05104 a.u.. This value compares well with the near-Hartree-Fock limit of -78.0616 a.u. [24]. The resulting orbital energies are -11.23132, -11.22958, -1.03735, -0.79638, -0.64629, -0.59183, -0.50945, and -0.37710 a.u. for the $1a_g$, $1b_{1u}$, $2a_g$, $2b_{1u}$, $1b_{2u}$, $3a_g$, $1b_{3g}$, and $1b_{3u}$ orbitals, respectively.

All matrix elements arising in the present calculations were evaluated using a single-center expansion truncated at l_{max} = 14. All allowed h values (h £ l) for a given l were retained. Increasing l_{max} in these expansions did not lead to any significant change in the resulting cross sections. The basis set used in the solution of Eq. (6) is given in Table 1. All cross sections shown below were converged within 4 iterations.

Table I: Basis sets used in separable potential

Photoionization Symmetry	Center	Type of Cartesian Gaussian Function[a]	Exponents
ka_g	C	s	8.0, 2.0, 0.5, 0.1, 0.02
		z	4.0, 1.0, 0.25, 0.05, 0.01
	H	s	2.0, 0.5, 0.1, 0.02
		z	4.0, 1.0, 0.25, 0.05
	CM	s	4.0, 1.0, 0.25, 0.05
ka_u	C	y	8.0, 2.0, 0.5, 0.12, 0.03
	H	y	4.0, 1.0, 0.25, 0.05, 0.01
kb_{1g}	C	y	8.0, 2.0, 0.5, 0.12, 0.03
	H	y	4.0, 1.0, 0.25, 0.05, 0.01
kb_{1u}	C	s	8.0, 2.0, 0.5, 0.1, 0.02
		z	4.0, 1.0, 0.25, 0.05
	H	s	2.0, 0.5, 0.1, 0.02
		z	4.0, 1.0, 0.25, 0.05
	CM	s	4.0, 1.0, 0.25, 0.05
kb_{2g}	C	x	8.0, 2.0, 0.5, 0.12, 0.03
	H	x	4.0, 1.0, 0.25, 0.05, 0.01
kb_{2u}	C	y	8.0, 2.0, 0.5, 0.12, 0.03
	H	y	4.0, 1.0, 0.25, 0.05, 0.01
	CM	y	4.0, 1.0, 0.25, 0.05, 0.01
kb_{3g}	C	y	8.0, 2.0, 0.5, 0.12, 0.03
	H	y	4.0, 1.0, 0.25, 0.05, 0.01
kb_{3u}	C	x	4.0, 1.0, 0.25, 0.05, 0.01
	H	s	2.0, 0.5, 0.1, 0.02
		x	4.0, 1.0, 0.25, 0.05
	CM	x	4.0, 1.0, 0.25, 0.05

[a] Cartesian Gaussian basis functions are defined as $f^{a,l,m,n}(\mathbf{A}(\mathbf{r}) = N(x-\mathbf{A}_x)^l (y-\mathbf{A}_y)^m (z-\mathbf{A}_z)^n \exp(-a|\mathbf{r}-\mathbf{A}|^2)$, with N a normalization constant. CM denotes the center of mass.

III. Results and Discussion

Figures 1 to 4 show our calculated photoionization cross sections and photoelectron angular distributions for ionization of ground state of ethylene leading to the X^2B_{3u} ($1b_{3u}^{(-1)}$), A^2B_{3g} ($1b_{3g}^{(-1)}$), B^2A_g ($3a_g^{(-1)}$) and C^2B_{2u} ($1b_{2u}^{(-1)}$) ionic states, respectively. Discussion of these results for each photoionization channel is presented separately below.

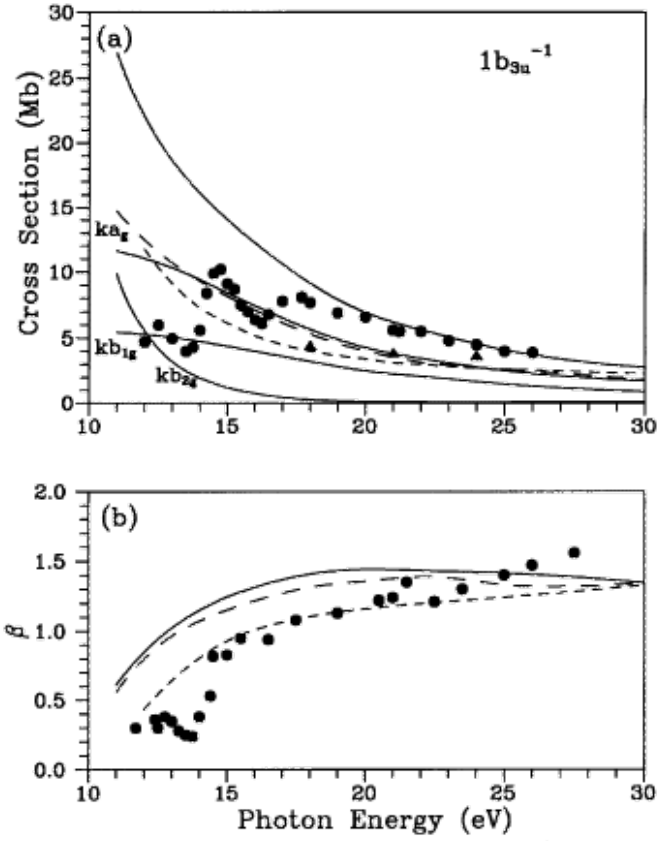

Figure 1. (a) Photoionization cross sections for the $X^2B_{3u}(1b_{3u}^{-1})$ state of $C_2H_4^+$. Solid line (length) and long-dashed line (velocity): present results; dashed line : results of Grimm (Ref. [19]); circles and triangles: experimental results from Refs. [15] and [16], respectively; solid lines with lables kb_{1g}, kb_{2g}, and ka_g: contributions of these channels to cross section (see text). (b) Photoionization asymmetry parameter for the $X^2B_{3u}(1b_{3u}^{-1})$ state of $C_2H_4^+$. Solid line (length) and long-dashed line (velocity): present results; dashed line: results of Grimm (Ref. [19); circles: experimental results of Ref. [17].

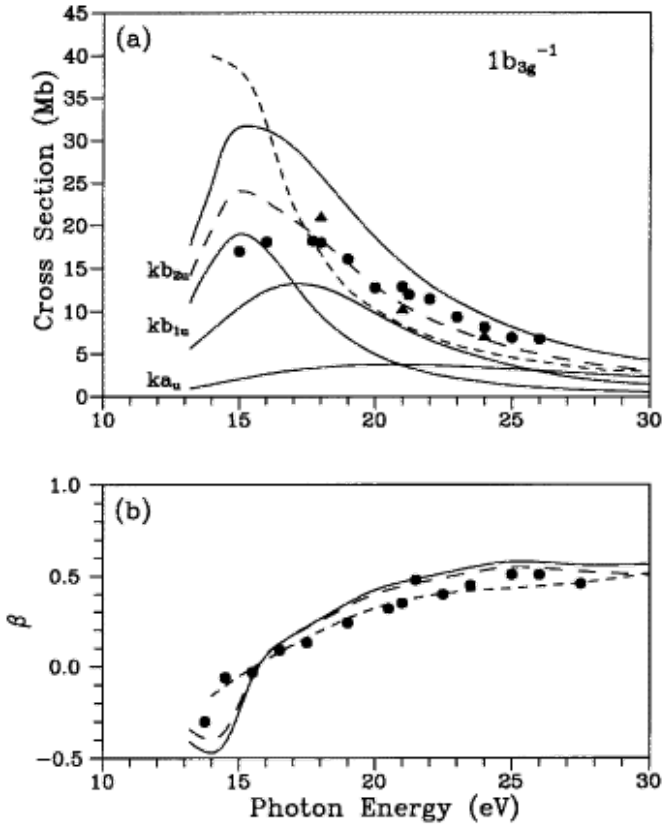

Figure 2. Same as Fig. 1 for the $A^2B_{3g}(1b_{3g}^{-1})$ state of $C_2H_4^+$.

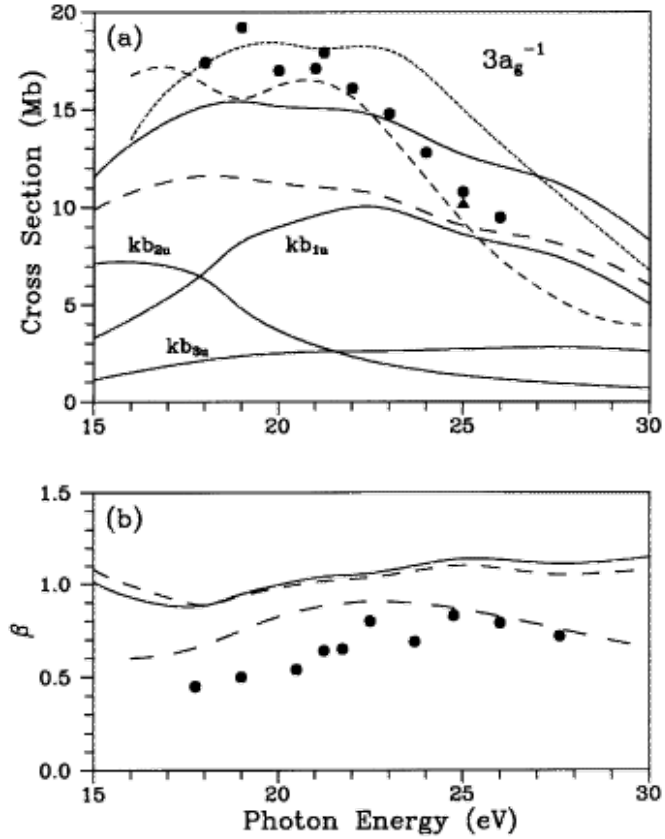

Figure 3. Same as Fig. 1 for the $B^2A_g(3a_g^{-1})$ state of $C_2H_4^+$. Here the calculated results of Farren *et al.* [21] are shown by the short-dashed line.

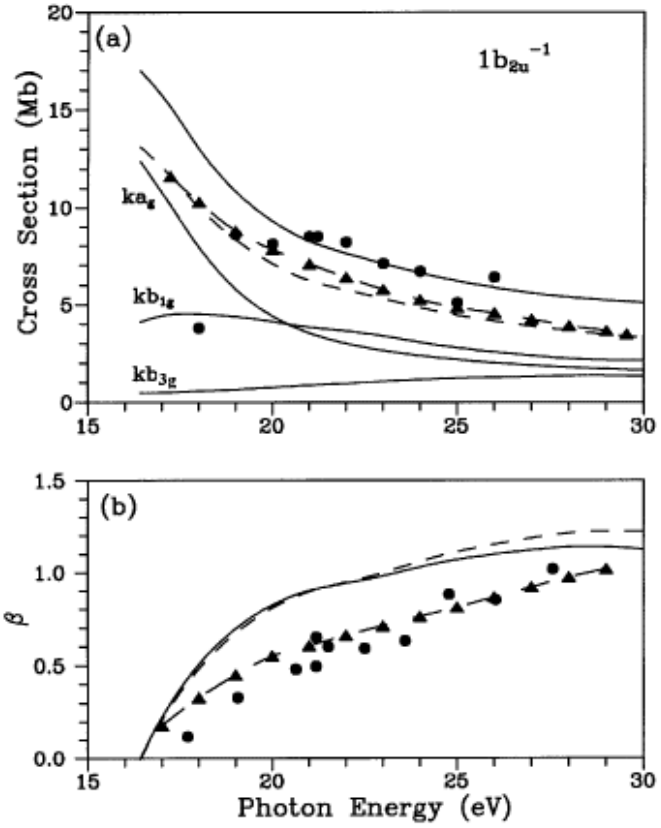

Figure 4. Same as Fig. 1 for the $C^2B_{2u}(1b_{2u}^{-1})$ state of $C_2H_4^+$.

1. $1b_{3u}$ **($p_{C\text{-}C}$, I.P. = 10.51 eV)**

Figure (1a) shows the calculated photoionization cross section for the $1b_{3u}$ orbital of ethylene along with the results of Grimm et al. [19] obtained using the continuum multiple-scattering method ($CMSX_a$) and some selected data obtained from synchrotron radiation measurements [15,16]. The individual contributions of the ka_g, kb_{1g}, and kb_{2g} partial channels, with the length form of the dipole operator, are also included in the figure. The differences between the dipole-length and dipole-velocity cross sections, as seen in the figure, are known to be generally due to the neglect of electron correlation in the wavefunction. Comparison between the present results and experimental data above 17 eV is encouraging. The structure seen around 12.5 and 14.5 eV in the experimental data is due to autoionizing resonances. Similar structures are observed in the photoionization of $1p_u$ orbital of C_2H_2 and have been interpreted previously [25]. Since our present formulation provides only the direct contribution to the photoionization cross section, any effect arising from autionization cannot be accounted for. A comparison of our results with the calculated $CMSX_a$ cross sections shows qualitative agreement. The $CMSX_a$ cross sections are in general smaller than our results at lower energies. The main difference comes from the contribution of the kb_{2g} channel which in the present calculation is important near threshold, in contrast to the $CMSX_a$ results. On the other hand, the STMT-RPA study of Galasso [20] (not shown to avoid clutter in the figure) reported a resonance-like peak in the photoionization cross sections at about 19 eV. This peak is neither seen in the present and $CMSX_a$ studies nor observed in the measured cross sections.

In Fig. (1b) we compare the calculated photoelectron angular distribution (b) with the corresponding $CMSX_a$ results [19] and with the synchrotron data of Mehaffy *et al*. [17]. Agreement between the calculated and measured results is in general good. The structure shown in the experimental data at lower energies is again attributed to autionization and is not reproduced in the calculations.

2. $1b_{3g}$ **(**s_{C-H}**, I.P. = 12.85 eV)**

Figure (2a) shows our calculated cross sections along with the $CMSX_a$ results of Grimm [19] and the measured data of Grimm *et al.* [15] and Brennan *et al.* [16]. The broad maximum in the cross sections around 16 eV is seen to arise from underlying resonance-like behavior in the kb_{2u} and kb_{1u} channels. The calculated results, mainly in dipole-velocity form, are in very good agreement with the experimental data. The eigenphase sum analysis of the partial channels does not support the existence of resonances near threshold, in contrast with the predictions of the STMT-RPA study of Galasso [20]. Indeed, the enhancements of the partial cross sections around 15 eV (kb_{2u}) and 17.5 eV (kb_{1u}) arise from *f* wave components of the photoelectron continuum. On the other hand, the calculated $CMSX_a$ cross sections of Grimm [19] show a continuous decrease from threshold.

Figure (2b) shows our calculated photoelectron angular distributions along with the experimentally determined b values and the CMSXa results of Grimm [19]. Again, agreement between calculated and experimental results is good.

3. $3a_g$ **(**s_{C-C}**, I.P. = 14.66 eV)**

Our calculated cross sections and photoelectron angular distributions for photoionization of the $3a_g$ orbital of ethylene are shown in Figs. (3a) and (3b), respectively, along with the experimental data of Grimm *et al.* [15] and Brennan *et al.* [16] and the calculated results of Grimm [19] and Farren *et al.* [21]. Here two broad maxima (around 16 eV and 23 eV) can be seen in the kb_{2u} and kb_{1u} photoionization channels, respectively. Thus, the resulting $3a_g^{-1}$ total cross sections also exhibit two broad maxima, in qualitative agreement with the calculated results of Farren *et al.* [21] and Grimm [19]. Again, for this photoionization channel, the enhancement of these partial cross sections is related to the energy dependence of the same (l = 3) components of the photoelectron continuum. In contrast, the STMT-RPA results of Galasso [20] (not shown) exhibit only one maximum around 16 eV. Above 23 eV, the experimental data lie between our dipole-length and dipole-velocity results. Our calculated photoelectron angular distribution agrees qualitatively with experimental data. Quantitatively, however, our calculated results lie above the experimental data over the entire energy range.

4. $1b_{2u}$ **(**s_{C-H}**, I.P. = 15.87 eV)**

The photoionization cross sections for the $1b_{2u}$ orbital of C_2H_4 are shown in Fig. (4a), along with experimental results of Grimm *et al.* [15] and the calculated CMSXa cross sections of Ref. [19]. There is a general agreement between our dipole-velocity results and the experimental data above 19 eV, as well as with the CMSXa results over the entire energy range. However, our dipole length cross sections lie systematically above the measured data over the entire energy range. Near threshold, a single experimental point at 18 eV shows a sudden drop in the cross sections, in contrast with our calculations. Unfortunately, due to the lack of additional data points in this energy region, no meaningful conclusion can be drawn from this disagreement. In Fig. (4b), we compare our photoelectron angular distributions with the experimental data and the CMSXa results. The qualitative agreement between calculated and experimental results is generally good, although our calculated b lies above the measured values.

IV. Concluding Remarks

We have reported cross sections and asymmetry parameters for the photoionization of the four outmost valence orbitals of ethylene, both in length and velocity forms. Due to the lack of correlation in our SCF calculation, the cross sections in the length form differ from those in the velocity form. The velocity form of these cross sections is generally in better agreement with the available experimental results. Similar conclusions were also reported by Lucchese *et al.* [9] in their study of the photoionization of the N_2 molecule. Indeed, the present study is the only that reports *ab initio* results for both partial cross sections and asymmetry parameters for photoionization of ethylene at the exact SE level. The eventual disagreement of our SE results and the experimental data could indicate that the inclusion of important effects beyond the SE level should be needed. On the other hand, a good agreement of semiempirical SE results with experiments for which the description in the SE approximation is expected to fail reveals that important physical effects are being masked in the calculations.

Acknowledgements

This research was partially supported by National Science Foundation, the Conselho Nacional de Desenvolvimento Cientí fico e Tecnológico (CNPq), FINEP-PADCT, CAPES-PADCT and FAPESP.

References

1. See, for example, S.T. Pratt, P.M. Dehmer, and J.L. Dehmer, Chem. Phys. Lett. **105**, 28 (1984). [Links]
2. W. Peatman, E.P. Wolf, and R. Unwin, Chem. Phys. Lett. **95**, 453 (1983). [Links]
3. S. W. Allendorf, D. J. Leahy, D.C. Jacobs, and R.N. Zare, J. Chem. Phys. **91**, 2216 (1989). [Links]
4. See, also, K. Wang and V. McKoy, Annu. Rev. Phys. Chem. **46**, 275 (1995) and references therein. [Links]
5. J. B. West, A. C. Parr, B. E. Cole, D. L. Ederer, R. Stockbauer and J. L. Dehmer, J. Phys. B: At. Mol. Phys. **13**, L105 (1980). [Links]
6. E. P. Leal, L. E. Machado and Mu-Tao Lee, J. Phys. B: At. Mol. Phys. **17**, L569 (1984). [Links]
7. H. Rudolph, J. A. Stephens, V. McKoy and M.-T. Lee, , J. Chem. Phys. **91**, 1374 (1989). [Links]
8. J. A. Stephens, M. Braunstein, V. McKoy, H. Rudolph and M.-T. Lee, , Physica Scripta **41**, 482 (1990). [Links]
9. R.R. Lucchese, G. Raseev, and V. McKoy, Phys. Rev. A **25**, 2572 (1982). [Links]
10. M. E. Smith, V. McKoy and R. R. Lucchese, J. Chem. Phys. **82**, 4147 (1985). [Links]
11. D. Lynch, M.-T. Lee, R. R. Lucchese and V. McKoy, J. Chem. Phys. **80**, 1907 (1984). [Links]
12. D. Lynch, S. N. Dixit and V. McKoy, J. Chem. Phys. **84**, 5504 (1986). [Links]
13. M. Braunstein, V. Mckoy, L. E. Machado, L. M. Brescansin, and M. A. P. Lima, J. Chem. Phys. **89**, 2998 (1988). [Links]
14. L. E. Machado, L. M. Brescansin, M. A. P. Lima, M. Braunstein, and V. Mckoy, J. Chem. Phys. **92**, 2362 (1990). [Links]
15. F.A. Grimm, T.A. Whitley, P.R. Keller and J.W. Taylor, (private communication).
16. J.G. Brennan, G. Cooper, J.C. Green, M.P. Payne and C.M. Redfern, J.Electron. Spectrosc. Relat. Phenom. **43**, 297 (1987).

[Links]

17. D. Mehaffy, P.R. Keller, J.W. Taylor, T.A. Carlson, M.O. Krause, F.A. Grimm and J.D. Allen Jr., J. Electron. Spectrosc. Relat. Phenom. **26**, 213 (1982).
[Links]

18. A.L.D. Kilcoyne, M. Schmidbauer, A. Koch, K.J. Randall and J. Feldhaus, J. Chem. Phys. **98**, 6735 (1993).
[Links]

19. F.A. Grimm, Chem. Phys. **81**, 315 (1983).
[Links]

20. V. Galasso, J. Mol. Struct. (Theo. Chem.) **168**, 161 (1988).
[Links]

21. R.E. Farren, J.A. Sheehy and P.W. Langhoff, Chem. Phys. Lett. **177**, 307 (1991).
[Links]

22. P. G. Burke, N. Chandra and F.A. Gianturco, J. Phys. B: At. Mol. Phys. **5**, 2212 (1972).
[Links]

23. T. H. Dunning Jr., J. Chem. Phys. **53**, 2823 (1970).
[Links]

24. E. Clementi and H. Popkic, J. Chem. Phys. **57**, 4870 (1972).
[Links]

25. P. W. Langhoff, V. McKoy, R. Unwin and A. Bradshaw, Chem. Phys. Lett. **83**, 270 (1981).

Caixa Postal 66328
05315-970 São Paulo SP - Brazil
Tel.: +55 11 3091-6922
Fax: (55 11) 3816-2063

e-Mail

sbfisica@sbfisica.org.br